A Numerical/Experimental Investigation of Microcontamination in a Rotating Disk Chemical Vapor Deposition Reactor

R. W. Davis*, E. F. Moore*, J. E. Maslar*, D. R. Burgess*, D. M. Kremer¶, and S. H. Ehrman¶

Chemical Science and Technology Laboratory, National Institute of Standards and Technology, Gaithersburg, MD 20899
¶*Department of Chemical Engineering, University of Maryland, College Park, MD 20742*

Abstract. Driven by a relentless decrease in feature size, the allowable particle contaminant size during semiconductor fabrication is now less than 100 nm. Particles in this size range (microcontaminants) in chemical vapor deposition (CVD) reactors are primarily gas-phase generated and are poorly understood. The purpose of the investigation described here is to enhance the understanding of the formation, transport and growth of microcontaminants in thermal CVD reactors. The approach being employed is to carry out a combined numerical/experimental study in which the particle dynamics are both modeled and optically probed in a rotating disk CVD reactor. The rotating disk configuration is utilized because of its simple and well-defined flow in which a particle layer forms in a highly accessible region of the reactor just above the substrate. Numerical/experimental comparisons of layer location and shape as a function of disk rotation rate are shown to be excellent if two empirically-determined parameters in the model are properly chosen.

INTRODUCTION

The 1999 International Technology Roadmap for Semiconductors [1] identifies the need for a more fundamental understanding of reactor contaminant formation, transport and deposition. It calls for the development and deployment of advanced chemistry/contamination models in order to provide defect-free process tools that predict failures/faults and automatically initiate corrective actions prior to defect formation. These needs are being driven by the relentless decrease in feature size. As feature size decreases, the allowable particle contaminant size also decreases. Upon attainment of the 100 nm technology node in 2005, the allowable particle size will only be 33 nm. The current understanding of particles in this size range (i.e., microcontaminants), which are gas-phase generated, is severely limited. The purpose of the investigation described here is twofold: to acquire an improved understanding of the behavior of microcontaminants in rotating disk thermal chemical vapor deposition (CVD) reactors; and to develop a predictive capability for their physics/chemistry in this type of reactor. The approach being employed is to carry out a combined numerical/experimental investigation in which the particle dynamics are both probed optically and simulated computationally. The rotating disk configuration is utilized because of its simple and well-defined flow in which a thin particle layer forms in a highly accessible region of the reactor just above the substrate. Numerical/experimental comparisons of this layer will be presented under conditions typical of silicon CVD. The behavior of the particle layer as disk rotation rate is varied will be discussed. Two empirical parameters in the model will be shown to control layer location and thickness. These parameters control the thermophoretic force and the probability of sticking during condensational particle growth. Proper selection of these parameters is demonstrated to result in excellent agreement between the numerical and the experimental results. Overlays of the simulated particle layers with the experimental layers at rotation rates of 500 rpm, 750 rpm, and 1000 rpm illustrate this agreement.

NUMERICAL MODEL

The numerical model employed here is based on the von Karman similarity transformation that reduces the central region of the reactor to a one-dimensional formulation above an infinite radius disk. The Sandia SPIN code [2] is utilized to compute the flow and chemistry, while a moment transport method based on a lognormal particle size distribution is employed for the aerosol dynamics. Particle nucleation, growth via coagulation and condensation, and transport due to convection, diffusion, thermophoresis and gravity are all considered. A complete description of the model is presented in Davis et al. [3]. Of particular note are two empirical parameters that determine the thermophoretic force on the particles and the sticking probability during condensational growth of the particles (see Appendix). The thermophoretic force is ascertained by a formula that is known to only approximately represent the true force [4,5]. The height of the particle layer above the susceptor increases as this force, which drives particles down a thermal gradient (i.e., upward here), increases. Thus, a final adjustment must be made based on the height of the experimental layer. The sticking probability during condensational growth is only known to lie somewhere between 0 and 1 [3]. The thickness of the particle layer varies inversely with this parameter, and thus it must also be determined based on experimental data. The resulting model is therefore semi-empirical in nature pending further advances in our basic understanding of aerosol dynamics in chemically reacting systems.

Computations are carried out on high performance workstations. Typical outputs from this model are particle number concentrations, size distributions, and optical scattering power. Reactor performance maps that indicate both film growth rate and substrate contamination rate as functions of disk temperature can also be derived from this model [3]. This paper will focus on comparisons of the simulated particle layers with those observed via light scattering in an experimental rotating disk CVD reactor.

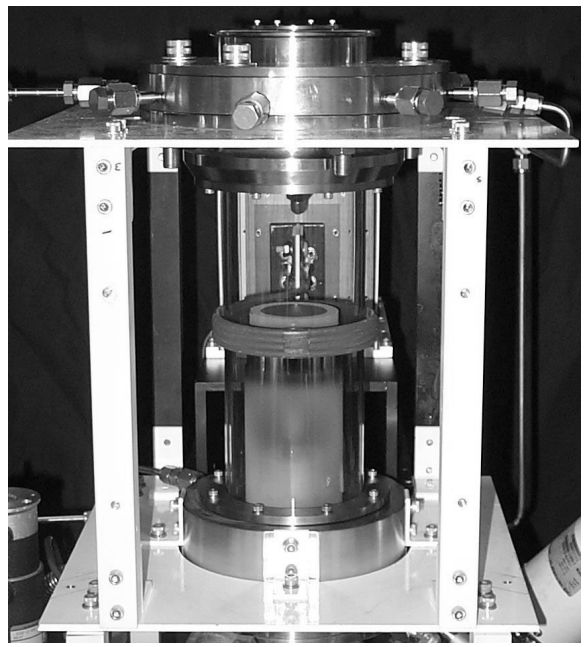

FIGURE 1. Photograph of the reactor.

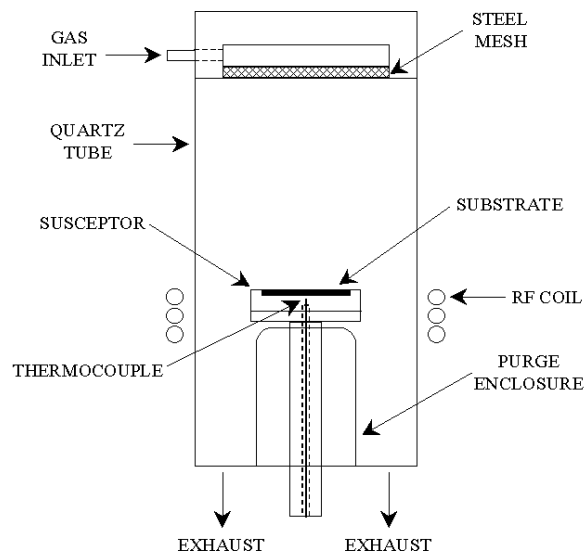

FIGURE 2. Schematic of the reactor.

EXPERIMENTAL TECHNIQUE

CVD Reactor

A photograph of the CVD reactor is shown in Fig. 1, and a schematic is shown in Fig. 2 (see [6] for performance details). The silicon precursor (silane) and the carrier gas (helium) are injected at the top, flow through a stainless steel mesh into the 10 cm internal diameter quartz tube, and are exhausted through the bottom of the reactor. A 5 cm diameter silicon wafer rests in the recess of a 6.7 cm diameter molybdenum susceptor which is inductively heated with a 5 kW RF power supply. The distance from the mesh to the susceptor is 15 cm. A chromel-alumel thermocouple in contact with the susceptor base is used in the control of the RF power supply output to maintain the thermocouple temperature to within ±1 K of the set point. Gas compositions of between 0.25 and 0.50 mole percent silane in helium are used at chamber pressures between 20.0 kPa (150 torr) and 66.7 kPa

(500 torr). Chamber pressure is measured with a capacitance manometer. A mass flow controller is used on each gas line to regulate gas flow rate.

Optical Measurements

Laser light scattering is used to image particles in the reactor. A laser sheet is formed by first expanding a 488 nm wavelength beam with a –25 mm focal length cylindrical lens and then focusing the light with a 500 mm focal length cylindrical lens. At the susceptor center, the sheet is approximately 100 mm high (maximum optical access) with a width of approximately 250 μm. The scattered light is collected with an imaging lens oriented at 90° to the direction of propagation of the laser sheet. The lens focuses the collected light onto a thermo-electrically cooled, back-illuminated, 2048 x 512 pixel array charge coupled device (CCD) camera. The individual CCD pixel size is 13.5 μm x 13.5 μm. The spatial resolution of the optical system is 332 pixels/cm, and the positional uncertainty is ± 1 pixel. A 488 nm interference filter is used before the lens to reject blackbody radiation. All images are obtained in integration times of 4 s or less.

RESULTS AND DISCUSSION

During thermal decomposition of silane, a particle layer is observed between 3 mm and 5 mm above the susceptor for all process conditions. Figure 3 shows a photograph of the reactor under typical silicon layer growth conditions with 0.50 mole percent silane injection in helium, 1100 K thermocouple temperature, 500 rpm nominal susceptor rotation rate, 20.0 kPa (150 torr) chamber pressure, and 13.0 slpm gas flow rate. The particle layer is clearly visible here. The properties of this layer, *e.g.*, height above the susceptor and thickness, varied as process conditions were changed.

Particle layers which formed with 0.25 mole percent silane injection in helium, 1100 K and 1150 K thermocouple temperatures, 26.7 kPa (200 torr) pressure, 19 slpm flow rate, and 500 rpm, 750 rpm, and 1000 rpm nominal rotation rates were imaged with the CCD camera. The layer position and thickness were then determined for each case. The layer heights are summarized in Table 1. It is apparent from these results that a 50 K change in temperature has much less effect on layer position than a 250 rpm change in susceptor rotation rate. The 50 K temperature variation merely results in a slight shift of the particle layer of approximately 0.1 mm. However, changes in rotation rate result in significant changes in the viscous boundary layer thickness above the susceptor surface. This boundary layer, which contains the thermal gradients driving particle formation, has a thickness that varies inversely with the square root of the rotation rate [7]. Thus, the height of the particle layer above the susceptor decreases as the susceptor rotation rate increases at constant temperature.

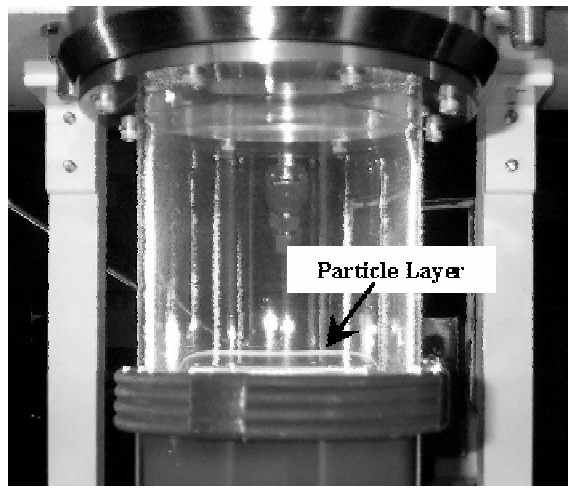

FIGURE 3. Photograph of reactor showing particle layer.

TABLE 1. Measured distance from the susceptor to the particle layer as a function of susceptor rotation rate and temperature. Positional uncertainty is ± 0.03 mm.

Susceptor Rotation Rate (rpm)	Susceptor-Layer Distance (mm)	
	Thermocouple at 1100 K	Thermocouple at 1150 K
500	5.64	5.76
750	4.86	4.94
1000	4.25	4.32

Numerical simulations were performed for process conditions corresponding to 0.25 mole percent silane injection in helium, 1100 K thermocouple temperature (assuming a susceptor surface temperature of 1050 K based on Raman gas-phase temperature data indicating a surface temperature slightly less than the embedded thermocouple temperature), 26.7 kPa (200 torr) pressure, 19 slpm flow rate, and 500 rpm, 750 rpm, and 1000 rpm rotation rates. Figures 4, 5, and 6 show the normalized experimental and numerical scattering intensity profiles for rotation rates of 500 rpm, 750 rpm, and 1000 rpm, respectively. The numerical profiles represent the sixth moment of the particle size distribution (see [3]). In all figures, the agreement between the experimental and numerical results is observed to be excellent. As noted previously, it was necessary to adjust the values of the thermophoretic

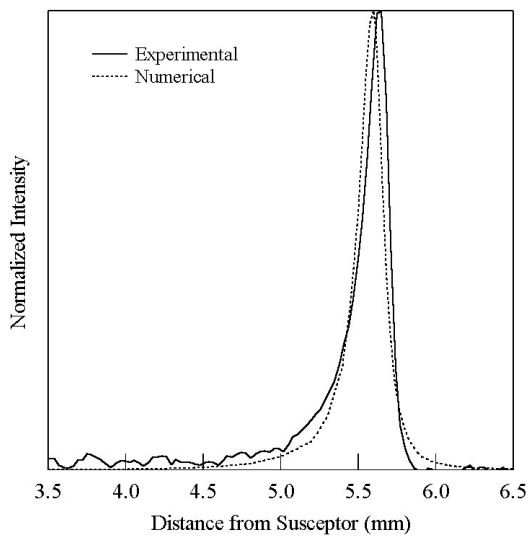

FIGURE 4. Numerical and experimental scattering intensity profiles as a function of height above the susceptor surface for a rotation rate of 500 rpm.

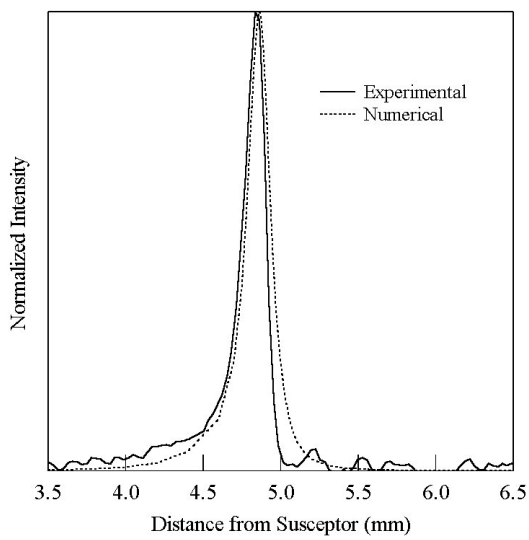

FIGURE 5. Numerical and experimental scattering intensity profiles as a function of height above the susceptor surface for a rotation rate of 750 rpm.

force coefficient, C_{th}, and the sticking probability, α, in Eqs. (1) and (2) in order to obtain this level of agreement. Table 2 lists the values of these parameters used to calculate the numerical results shown in the figures. As can be seen, the thermophoretic force coefficient varies only slightly from 1.6 at 500 rpm to 1.8 at 750 rpm and 1000 rpm. Given the uncertainties inherent in the calculation of the thermophoretic force [4,5], these values for this coefficient are not

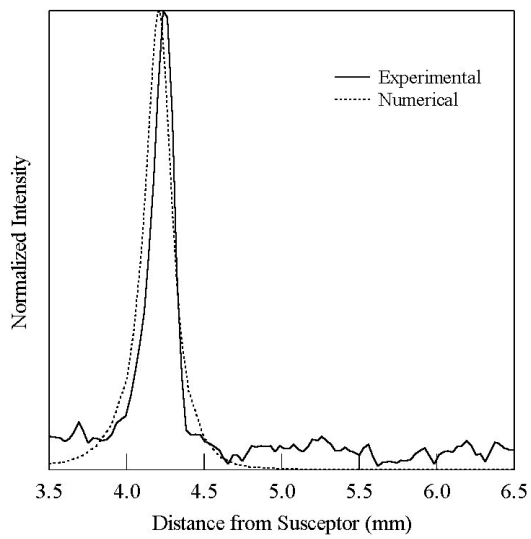

FIGURE 6. Numerical and experimental scattering intensity profiles as a function of height above the susceptor surface for a rotation rate of 1000 rpm.

TABLE 2. Values of thermophoretic force coefficient and sticking probability used in the model.

Susceptor Rotation Rate (rpm)	Thermophoretic Force Coefficient C_{th}	Sticking Probability α
500	1.6	0.030
750	1.8	0.065
1000	1.8	0.100

unreasonable. All sticking probabilities are less than or equal to 0.10. More investigation will be required in order to determine the reason for the increased probability with rotation rate. A full sensitivity analysis has not yet been performed. However, it appears that the relative changes in calculated layer height are less than the relative changes in C_{th}, while relative changes in calculated layer thickness are several times the relative changes in α.

The excellent agreement between simulation and experiment observed in Figs. 4-6 relates to particle layer vertical height and shape but not intensity. Each profile is normalized with respect to its own peak value. There is as yet no clear procedure to quantitatively compare numerical and experimental peak intensities. Future work will focus on performing both this quantitative comparison as well as comparing predicted and actual particle sizes and number concentrations. The numerical model generates spatial

profiles throughout the boundary layer of average particle size and number concentration. Typical peak values of predicted particle size are 10 nm to 30 nm at a number concentration of approximately 10^{10} particles/cm^3. Full validation of the model will require these predictions to be verified experimentally.

CONCLUDING REMARKS

A numerical/experimental investigation of particle dynamics in a rotating disk CVD reactor is currently underway. An aerosol dynamics model is being utilized to simulate the formation, growth, and transport of microcontaminants during process conditions typical of silicon CVD. Optical diagnostics are being employed to probe gas-phase particle behavior in an experimental reactor apparatus for comparison with the numerical results.

The excellent agreement between simulation and experiment reported here indicates that the model is correctly accounting for the essential features of the physics/chemistry of the aerosol. Because of significant gaps in our understanding of some of the underlying factors driving the aerosol dynamics, it has been necessary to employ two empirical parameters in the model. Thus experimental validation of this model becomes more complex than simply verifying the predictions. Values for the empirical parameters must also be determined that can be utilized over as wide a range of process conditions as possible. In addition, it is desirable that these parameters do not exhibit highly variable (i.e., orders of magnitude variation) behavior as process conditions are altered within this range. From the results presented here, this does in fact appear to be the case.

Finally, it is clear that the existence of a particle layer during silicon CVD in this type of reactor has implications for both efficiency and quality control during semiconductor fabrication. The formation of this particle layer consumes a portion of the silane precursor, thereby limiting the growth rate of the film on the substrate. Particles may also be diffusing from this layer to the substrate, thus representing a source of contamination. The extent of both of these potential problems in actual fabrication reactors will require further investigation.

ACKNOWLEDGMENTS

The authors gratefully acknowledge Prof. M. R. Zachariah of the Department of Mechanical Engineering, University of Minnesota and Dr. C. A. Wang of Lincoln Laboratory, Massachusetts Institute of Technology for helpful discussions. Mr. R. R. Fink of NIST assisted in assembly and operation of the experimental CVD reactor.

REFERENCES

1. "The International Technology Roadmap for Semiconductors," Semiconductor Industry Association, 1999.
2. Coltrin, M. E., Kee, R. J., Evans, G. H., Meeks, E., Rupley, F. M., and Grcar, J. F., "SPIN (Version 3.83): A FORTRAN Program for Modeling One-Dimensional Rotating-Disk/Stagnation-Flow Chemical Vapor Deposition Reactors," Sandia National Laboratories Report SAND91-8003, 1991.
3. Davis, R. W., Moore, E. F., Burgess, D. R., and Zachariah, M. R., "A Microcontamination Model for Rotating Disk Chemical Vapor Deposition Reactors," in *Characterization and Metrology for ULSI Technology*, edited by D. G. Seiler et al., AIP Conference Proceedings 449, New York, 1998, pp. 918-922.
4. Whitby, E. R., McMurry, P. H., Shankar, U., and Binkowski, F. S., "Modal Aerosol Dynamics Modeling," U. S. Environmental Protection Agency Report for Contract No. 68-01-7365, 1991.
5. Hinds, W. C., *Aerosol Technology*, John Wiley, New York, 1982, pp. 153-157.
6. Biber, C. R., Wang, C. A., and Motakef, S., *J. Crystal Growth* **123**, 545-554 (1992).
7. Breiland, W. G., and Evans, G. H., *J. Electrochem. Soc.* **138**, 1806-1816 (1991).

APPENDIX

The thermophoretic force on a particle in the transition and free-molecular regimes that is utilized here is:

$$F_{th} = - C_{th} P \lambda d_p^2 \nabla T / T, \qquad (1)$$

where C_{th} is the empirical thermophoretic force coefficient, P is the reactor pressure, λ is the mean free path of the gas molecules, d_p is the particle diameter and T is the gas temperature.

The condensational volume growth rate of a particle is:

$$dv_p /dt = \alpha P \pi d_p^2 v_m / (2 \pi m k_B T)^{1/2} , \qquad (2)$$

where v_p is the particle volume, t is time, α and m are the empirical sticking probability and the mass of the condensible species molecules (e.g., Si_2H_2), v_m is the molecular volume of the condensed phase (e.g., Si), and k_B is the Boltzmann constant.